A Nature Portfolio journal



https://doi.org/10.1038/s42003-025-08165-x

Early life stress impairs hippocampal subfield myelination

Check for updates

Emily S. Nichols **®** ^{1,2} ⊠, Bradley G. Karat³, Michael Grace⁴, Samantha Bezanson⁵, Ali R. Khan², & Emma G. Duerden¹, 2,3,6,7</sup>

The hippocampus is an archicortical structure that is highly sensitive to experience and is made up of individual subfields. These subfields, crucial for learning and memory, rapidly develop and are vulnerable to early stress, yet the mechanisms are unknown. Here, we analyse data from 520 neonates born between 23 and 42 weeks' gestation to assess how early extrauterine exposure-related stress influences subfield maturation. Subfields are segmented automatically by training a U-net model on infant data using HippUnfold, a novel tool for subfield segmentation. Results indicate that subfield volumes are resilient to early stress, while myelination shows greater vulnerability and variation, which may contribute to long-term outcomes. Notably, subfields are not uniformly impacted by stress, with CA1 and CA2 showing the largest effects. Developmental context, including time spent *in* and *ex utero*, primarily influences hippocampal subfield myelination.

The hippocampus is a highly adaptable archicortical structure that develops slowly throughout early life^{1,2}. Cognitive and affective processes, including memory, spatial processing, emotion, motivation, and language are dependent on normal hippocampal development^{3–6}, which is highly sensitive to experience and particularly early stress⁷, such as environmental adversity. Alterations in hippocampal structure and function have been linked to several developmental disorders including attention-deficit/ hyperactivity disorder, autism spectrum disorder, and obsessive-compulsive disorder⁸. Importantly, the hippocampus is highly sensitive to experience; volumes in term-born infants increase exponentially after birth², and both its structure and function are affected by stress and childhood adversity^{9–11}. Nevertheless, the neurobiological mechanisms underlying this vulnerability remain unknown.

Anatomically, the hippocampus is a unique grey matter structure with a complex folding pattern. The hippocampal grey matter is made up of distinct subfields, comprising the cornu ammonis (CA1-4), the dentate gyrus (DG), and the subiculum, each with their own function, structure, and connectivity, with several subfields showing nonlinear growth in childhood¹². In children, research has demonstrated variability in subfield volumes related to different developmental disorders and stressors⁷, however, results are mixed in terms of the specific subfields involved and the direction of the effects¹³⁻¹⁵. The bulk of the white matter of the hippocampus is contained within the subiculum as the perforant path and within the

stratum radiatum lacunosum moleculare (SRLM) layers; however, it is also present in the dentate gyrus and hippocampus proper ^{16,17}, and studies have revealed varying patterns of myelination throughout the brain in neonates ^{18,19}. In contrast to volumes, although hippocampal myelination has been implicated in psychiatric disorders in adults ^{20,21}, it is understudied in general, especially in developmental samples. Hippocampus developmental timelines differ substantially between volume and myelination, with volumetric development occurring primarily in the first trimester and myelination occurring primarily in the third trimester ^{21,22}. Therefore, hippocampal subfield myelination may be more vulnerable to stress from early exposure to the extrauterine environment seen in preterm birth.

The postnatal period that corresponds to the third trimester in preterm infants has been characterized as a period of significant adversity²³, with much disruption to the still maturing brain and its development. Evidence from humans and animal models has indicated that both sensory regions and areas sensitive to stress, such as the hippocampus, amygdala, and insula, are regulated by input from the environment, and premature exposure to the extrauterine environment can interrupt developmental trajectories in stress-sensitive networks^{24–27}. Here, we investigated the effect of early life stress on volumetric and myelin development in the hippocampal subfields, using preterm birth as a model. We analyzed data from 520 newborn infants from the Developing Human Connectome Project²⁸, 120 of which were born preterm. We compared both grey matter volume and T1w/T2w ratio

¹Faculty of Education, Western University, London, ON, Canada. ²Western Institute for Neuroscience, Western University, London, ON, Canada. ³Robarts Research Institute, Schulich School of Medicine and Dentistry, Western University, London, ON, Canada. ⁴Physiology and Pharmacology, Schulich School of Medicine and Dentistry, Western University, London, ON, Canada. ⁵Neuroscience program, Schulich School of Medicine & Dentistry, Western University, London, ON, Canada. ⁶Medical Biophysics, Schulich School of Medicine & Dentistry, Western University, London, ON, Canada. ⁷These authors contributed equally: Ali R. Khan, Emma G. Duerden. ⊠e-mail: enicho4@uwo.ca

as a proxy for myelin between preterm- and term-born neonates to determine whether early stress differentially affects their development. We began by extending the existing HippUnfold automated subfield segmentation tool²⁹ for use in newborns, by training new machine learning models and adapting the workflow for neonatal MRI data. Subfield volumes were extracted, and myelination was assessed by way of T1w/T2w ratio in the hippocampal gray matter³⁰. By comparing the predictive power of each model, we determined whether volumes and myelination were sensitive to preterm birth. We then replicated our findings in a withheld sample of 25 preterm-born infants from the dHCP dataset who had both a scan at birth (that is, earlier than 37 weeks) and at term equivalent age (approximately 40 weeks). We compared both ages to 25 age- and sex-matched term-born infants, revealing differences in how predictive the stress models were, and how stress-exposed infants developed in terms of volumes and myelination.

Results

We successfully segmented the hippocampus using the T1-weighted images, using an incremental U-net training approach. An existing HippUnfold model trained on adult hippocampi with a contrast-agnostic approach (described in the online methods) was first applied to the neonatal T1-weighted data, also employing a neonatal T1-weighted template for initial linear image registration. Successfully segmented cases were then used to train subsequent models that employed the neonatal T1-weighted images. Final segmentations were graded for segmentation quality by multiple

raters, and did not differ in quality with respect to hemisphere (X^2 (1, N = 1250) = 1.41, p = 0.235). Volumes for each subfield were calculated in native space, and T1w/T2w ratio was averaged across subfield in unfolded space²⁹.

Two linear mixed models were then constructed. The first included postmenstrual age (i.e., age since conception) alone, modeling linear development with age. The second included both time spent in utero and ex utero, accounting for preterm birth. Importantly, both models account for total age of the infant, which is expected to be an important predictor of both volumes and myelination. All subfield volumes showed a clear increase in size with postmenstrual age, with CA1, CA3, and CA4/DG having a quadratic fit (Fig. 1A). The stress model, which includes both time spent in and ex utero, was better at predicting hippocampal subfield volumes than the age model, which considered postmenstrual age since conception alone, with greater explained variance and smaller error values (Volumes, Actual R² and MSE values, Table 1). However, differences in explained variance between models were small, ranging from less than 0.1% to 3%, which suggests that performance between the models was similar. Actual adjusted R² values in the stress model varied greatly across subfields, ranging from 0.12 in CA2 to 0.45 in CA4/DG, showing that volumetric sensitivity to stress was not uniform across subfields. Importantly, we tested whether this model could accurately predict volumes in a withheld sample of preterm (which included two timepoints, one during the preterm period and one at term equivalency) and term-born infants. Surprisingly, the age model

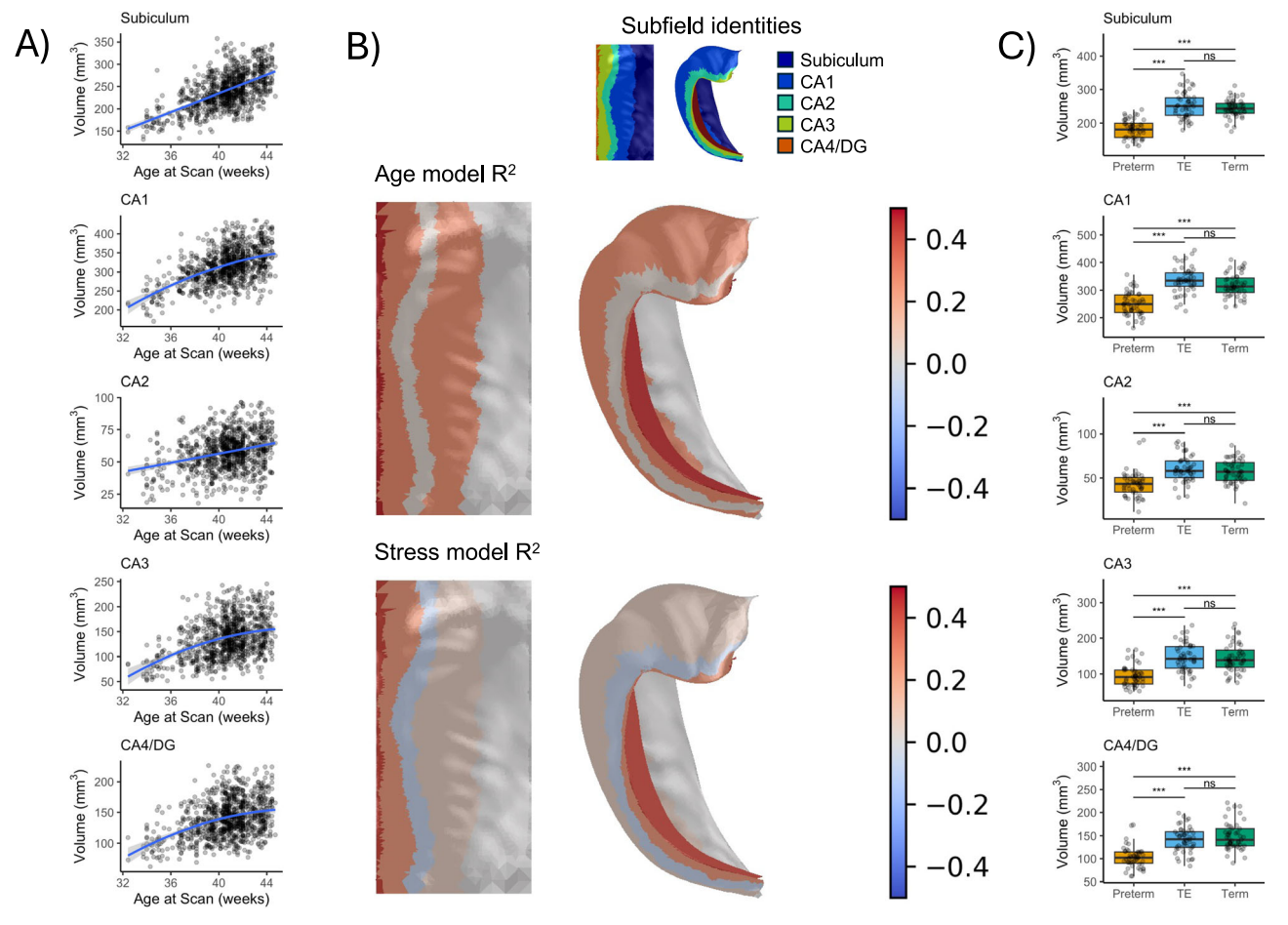


Fig. 1 | Hippocampal subfield volumes showed greater sensitivity to age compared to early stress. A The relationship between subfield volumes (y-axis) and age (x-axis). B Segmentation of hippocampal subfield volumes was performed using an iterative approach, with a group-based neonatal template for initial registration before being labeled and unfolded. Colours represent the R^2 values for the age (top) and stress (bottom) models, showing the model fit across the hippocampus. Warm colours indicate higher R^2 values, while cooler colors show lower model fit.

C Subfield volumes in preterm-born, term-equivalent preterm-born, and term-born infants. Medians are indicated by thick black horizontal lines. The first and third quartiles are marked by the lower and upper edges of the boxes, respectively. Lower and upper whiskers extend to the smallest and largest value, respectively, within 1.5 times the interquartile range. Outlying values beyond these ranges are plotted individually. CA cornu ammonis, DG dentate gyrus, TE term equivalent.

Table 1 | Actual and predicted adjusted R² and MSE values of postmenstrual age and stress models on hippocampal subfield volume and myelination

Measure	Data	Model		Subfields						
				Subiculum	CA1	CA2	CA3	CA4/DG		
Volumes										
	Actual	Age	R ²	0.39	0.39	0.10	0.35	0.42		
			MSE	1058.09 (954.76, 1161.42)	1330.93 (1197.56, 1464.31)	189.93 (172.35, 207.51)	1011.37 (918.62, 1104.11)	569.25 (514.68, 623.82)		
		Stress	R ²	0.42	0.42	0.12	0.35	0.45		
			MSE	1058.24 (947.83, 1168.66)	1261.69 (1134.98, 1388.40)	189.62 (171.79, 207.45)	1005.31 (912.99, 1097.63)	532.09 (480.88, 583.30)		
	Predicted	Age	R ²	0.17	0.25	0.03	0.27	0.46		
		Stress	R ²	< 0.01	0.06	-0.07	0.23	0.41		
Myelination	n									
	Actual	Age	R ²	0.30	0.16	0.11	0.21	0.26		
			MSE	0.014 (0.013, 0.016)	0.018 (0.017, 0.020)	0.033 (0.030, 0.036)	0.016 (0.015, 0.018)	0.015 (0.013, 0.016)		
		Stress	R ²	0.33	0.25	0.20	0.24	0.31		
			MSE	0.014 (0.012, 0.015)	0.017 (0.015, 0.018)	0.030 (0.027, 0.033)	0.016 (0.014, 0.017)	0.014 (0.012, 0.015)		
	Predicted	Age	R ²	-0.07	-0.07	-0.05	-0.02	-0.05		
		Stress	R ²	0.06	0.23	0.25	0.08	0.07		

CA cornu ammonis, DG dentate gyrus, MSE mean squared error.

outperformed the stress model in this replication sample (Predicted R^2 values, Table 1 and Fig. 1B), meaning that while prenatal and postnatal stress factors are relevant, postmenstrual age alone was a better predictor of volumes than stress in new, unseen data. Differences in explained variance between models were much larger, with the age model outperforming stress by 4–19%. Preterm volumes were notably smaller than those at term equivalency and in term-born infants (all p < 0.001, Table 2), but no significant differences were observed between term-equivalent and term-born volumes (all p > 0.05, Fig. 1C).

T1w/T2w ratio in the subfields also increased significantly with age, with all subfields having a quadratic fit, indicating that myelination slowed at approximately term age (Fig. 2A). However, the results observed in levels of myelination of the subfields followed a very different pattern from volumes. The stress model led to higher adjusted R² values in all subfields relative to the age model, ranging from 0.20 in CA2 to 0.33 in the subiculum, again indicating that the effect of stress on myelination is not uniform across the subfields (Myelination, Actual R² and MSE values, Table 1). Differences in explained variance between models were moderate, with the stress model outperforming age by 3-9%. When using each model to predict the withheld data, the stress model still provided better predictive value of myelination, greatly outperforming the age model with improvements in explained variance ranging from 10 to 30% (Myelination, Predicted R2, Table 1 and Fig. 2B). Comparing subgroups of the withheld sample also revealed that term-born infants had significantly higher levels of myelination than preterm-born infants both at birth and at term equivalency (all p < 0.006, Fig. 2C and Table 2).

Discussion

In examining the effects of early stress on hippocampal subfield maturation, two key points emerged: subfield volumes are relatively resilient to early life stress, while myelination is quite sensitive. Additionally, the pattern of early stress-related myelination changes was not uniform across subfields; while CA3 showed a relatively small (that is, 3%) difference between models, CA1 showed greater sensitivity with upwards of 25% of their variance in myelination being explained by preterm birth—9% more than age alone. We propose that the differences in stress susceptibility emerge from the structural properties of each subfield; prior work in adults has shown that CA3 has a greater myelin content than CA1^{29,31}, thus it appears that subfields with less myelination are more vulnerable to stress. CA1 is heavily involved

in episodic memory³², and variations in its structure have been associated with mood disorders³³. The connection between episodic memory and mood disorders has been well-established³⁴, and both are known to be impacted by preterm birth³⁵. Thus, the association of mood disorders with early life stress, including preterm birth, may reflect delayed or disrupted myelination of subfields mediating episodic memory. In contrast, volumes were more variably impacted by early stress, which may explain the conflicting results on the effects of preterm birth on subfield volumes in prior literature¹³⁻¹⁵.

Although the mechanisms remain unclear, the link between early life stress, the hippocampus, and enduring developmental outcomes into adulthood have been well-established. The results presented here provide a potential mechanism for this association, particularly when considering both the structure and function of the hippocampal subfields and how early stress shows a variable relationship with each. Findings further suggest that hippocampal subfields exhibit unique myelination compared to other white matter tracts that support broader connectivity, and less variable myelination patterns¹⁹. The hippocampus' specialized function and organization into subfields may result in different myelination needs and sensitivities, especially in response to early life stress.

Methods Participants

This research was performed using preprocessed data from the third release of the Developing Human Connectome Project (dHCP; obtained from http://www.developingconnectome.org/)^{28,36}. The dHPC is a large open science project of early life development lead by teams at King's College London, Imperial College London, and Oxford University, and includes imaging, genetic, demographic, and behavioural data for over 1000 infants and their parents. The infant imaging data used in the present study were collected between December 2014 and May 2020. Inclusion criteria were: Gestational age between 23- and 44-weeks, estimated from the mother's last menstrual period and confirmed where possible by early ultrasound scanning. Exclusion criteria were: Infants with contraindication to MR imaging, including implanted metallic devices such as orthopedic devices or noncompatible clips to close patent ductus arteriosus, preterm infants who are too unwell to tolerate the scanning period, despite full intensive neonatal care, and language difficulties preventing proper communication about the study and the consent process. The original study was approved by the

Table 2 | Estimated marginal effects comparing preterm- and term-born infant volumes and T1w/T2w ratio values in the longitudinal sample

Measure	Comparison	Subfield	Estimate	t(df)	р	95% CI
Volumes	Term-term equivalent	Subiculum	-9.89	-1.33 (60.8)	0.386	(-27.8, 8.0)
		CA1	-19.2	-2.02 (63.2)	0.117	(-42.0, 3.7)
		CA2	-3.06	-0.95 (68.6)	0.611	(-10.8, 4.67)
		CA3	-0.82	-0.10 (56.7)	0.994	(-20.2, 18.5)
		CA4/DG	6.65	1.31 (60.7)	0.398	(-5.6, 18.9)
	Term-preterm	Subiculum	60.98	8.18 (60.8)	< 0.001	(43.1, 78.9)
		CA1	67.3	7.07 (63.2)	< 0.001	(44.4, 90.1)
		CA2	13.86	4.28 (69.3)	< 0.001	(6.1, 21.6)
		CA3	52.13	6.50 (56.3)	< 0.001	(32.8, 71.4)
		CA4/DG	46.37	9.10 (60.7)	< 0.001	(34.1, 58.6)
	Term equivalent-preterm	Subiculum	70.87	14.93 (96.2)	< 0.001	(59.2, 82.5)
		CA1	86.4	13.03 (96.5)	< 0.001	(70.6, 102.2)
		CA2	16.92	6.75 (95.7)	< 0.001	(11.0, 22.9)
		CA3	52.95	11.63 (93.9)	< 0.001	(42.1, 63.8)
		CA4/DG	39.72	11.91 (96.2)	< 0.001	(31.8, 47.7)
T1w/T2w ratio	Term-term equivalent	Subiculum	0.13	4.20 (57.0)	< 0.001	(0.05, 0.20)
		CA1	0.17	5.65 (56.6)	< 0.001	(0.10, 0.24)
		CA2	0.23	4.67 (56.5)	< 0.001	(0.11, 0.34)
		CA3	0.11	3.16 (59.4)	0.007	(0.03, 0.19)
		CA4/DG	0.10	3.48 (57.5)	0.003	(0.03, 0.18)
	Term-preterm	Subiculum	0.31	10.46 (57.0)	< 0.001	(0.24, 0.39)
		CA1	0.31	10.29 (56.2)	< 0.001	(0.24, 0.38)
		CA2	0.35	7.35 (56.0)	< 0.001	(0.24, 0.47)
		CA3	0.29	8.27 (58.4)	< 0.001	(0.20, 0.37)
		CA4/DG	0.29	9.58 (57.5)	< 0.001	(0.21, 0.36)
	Term equivalent-preterm	Subiculum	0.19	10.82 (95.8)	< 0.001	(0.15, 0.23)
		CA1	0.14	8.15 (94.8)	< 0.001	(0.10, 0.18)
		CA2	0.13	4.75 (93.9)	< 0.001	(0.06, 0.19)
		CA3	0.18	8.13 (94.3)	< 0.001	(0.12, 0.23)
		CA4/DG	0.18	10.32 (95.8)	< 0.001	(0.14, 0.23)

CA cornu ammonis, DG dentate gyrus.

United Kingdom Health Research Authority (Research Ethics Committee reference number: 14/LO/1169) and written parental consent was obtained in every case for imaging and open data release of the anonymized data.

This release contained data for 887 sessions for 783 infants, and 638 infants had both T1- and T2-weighted anatomical images. Six MRI scans were performed under sedation, and 881 were not. After performing segmentation and data cleaning (described below) and removing participants with a diagnosis of growth restriction, gestational diabetes, pre-eclampsia, HELLP, or hypertension (78 infants), a final sample of 520 participants was analyzed (three acquired with sedation), and full participant demographics and clinical characteristics are shown in Table 3. Data were divided into two groups: (i) those participants with a single time point (the cross-sectional sample, 470 infants: 95 preterm, 375 term) and (ii) those with two time points (the longitudinal sample, 25 preterm infants), as well as a group of 25 term-born infants matched to the preterm group in sex and age at the term equivalent scan, who were withheld from the cross-sectional sample.

Magnetic resonance imaging

The T1-weighted anatomical images were acquired using an IR (Inversion Recovery) TSE sequence with TR = 4.8 s, TE = 8.7 ms, SENSE factor 2.26 (axial) and 2.66 (sagittal) with overlapping slices (resolution (mm) $0.8 \times 0.8 \times 1.6$). T2 images were obtained using a Turbo Spin Echo (TSE)

sequence with the same resolution, acquired in two stacks of 2D slices (in sagittal and axial planes), using parameters: TR = 12 s, TE = 156 ms, SENSE factor 2.11 (axial) and 2.58 (sagittal). Data were acquired on a Philips Achieva 3 T scanner at the Evelina Newborn Imaging Centre using a dedicated 32-channel neonatal head coil²⁸. All anatomical volumes were collected as part of the dHCP and are described in detail in Makropoulos et al.³⁷. The resulting images were motion corrected as described in Cordero-Grande et al.³⁶ and super-resolution reconstruction was performed as in Kuklisova-Murgasova et al.³⁸, resulting in 3D volumes resampled to 0.5 mm isotropic resolution. The resulting images were also corrected for bias field inhomogeneities.

Subfield segmentation with HippUnfold

HippUnfold is a novel tool for subfield segmentation, surface generation, and unfolding of the hippocampus. The first step of HippUnfold is a coarse affine registration to a template where a bounding box around the hippocampus is defined. Using this bounding box, the image is cropped around the hippocampus and rotated into a coronal oblique space. The cropped and coronal oblique images are then supplied to one of the core processes of HippUnfold: a deep neural network called nnU-Net³⁹ to segment the hippocampal gray matter and the boundaries of the hippocampus along orthogonal directions in participant space. The boundary regions include the hippocampal-amygdala transition area, medial temporal lobe cortex,

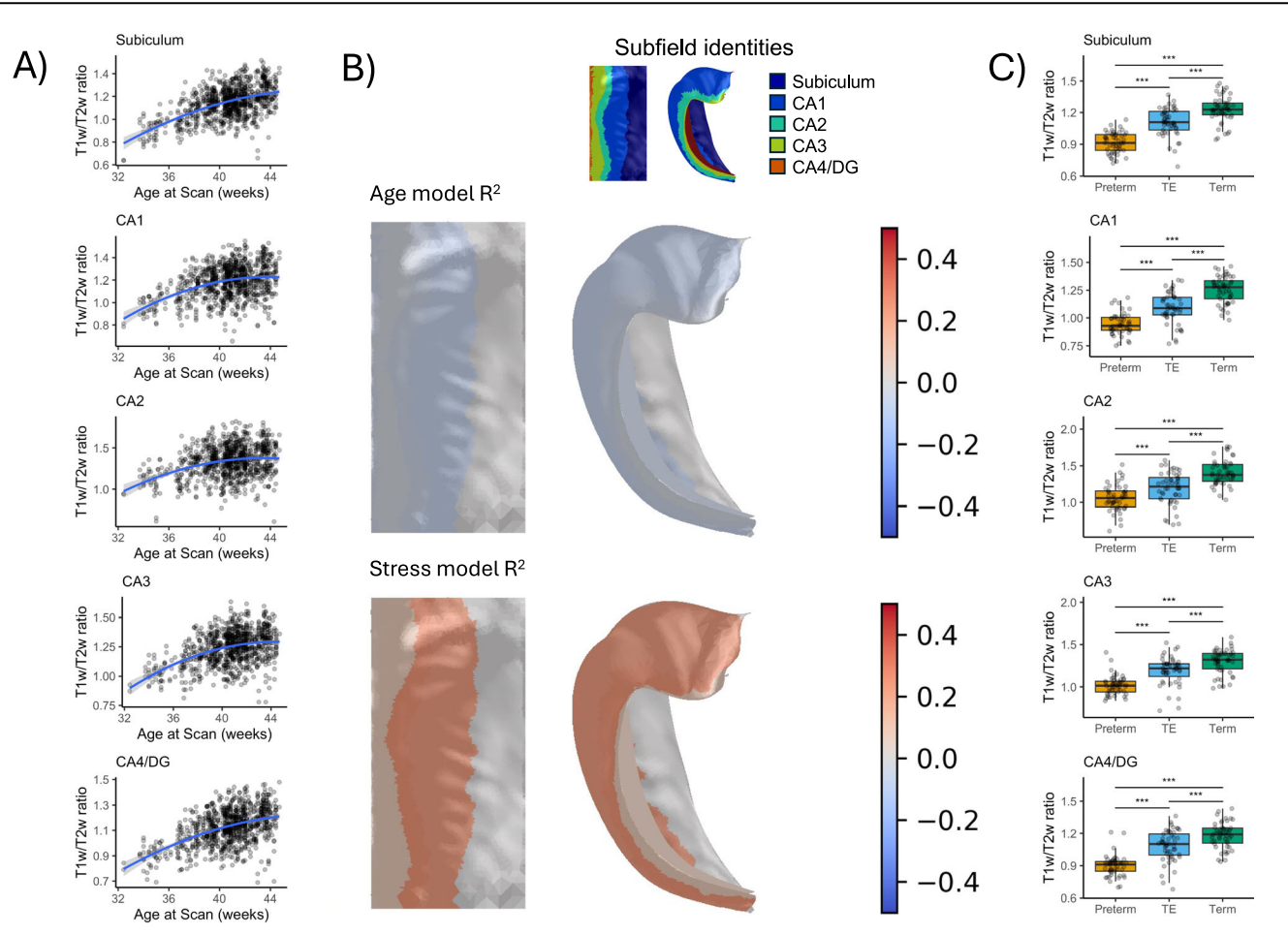


Fig. 2 | Hippocampal subfield myelination showed greater sensitivity to early stress than age. A The relationship between myelination (T1w/T2w ratio, y-axis) and age (x-axis). B The stress model showed better predictive power in a new dataset (R^2 values, warmer colors), than near-zero effect in the age model (R^2 values, cooler colours). C Subfield myelination in preterm-born, term-equivalent preterm-born, and term-born infants. Medians are indicated by thick black horizontal lines. The

first and third quartiles are marked by the lower and upper edges of the boxes, respectively. Lower and upper whiskers extend to the smallest and largest value, respectively, within 1.5 times the interquartile range. Outlying values beyond these ranges are plotted individually. CA cornu ammonis, DG dentate gyrus, TE term equivalent.

pial surface, stratum radiatum lacunosum moleculare (SRLM), and the indusium griseum. Using the boundaries of this participant-specific segmentation, a coordinate system is defined along the domain of the gray matter across the proximal-distal, anterior-posterior, and inner-outer hippocampal axes via solving Laplace's equation for these three axes independently. These coordinates have been demonstrated to have topological correspondence between variably shaped hippocampi, and we can use these coordinates to generate non-linear transformations between the native space and a canonical unfolded hippocampal space. Thus, we can project subfields from this unfolded space defined via histology (using the BigBrain dataset) into each subject's native space. We also generate surfaces at varying laminar depths in the unfolded space, and warp these into subject native space, enabling us calculate measures of gyrification, thickness, and curvature on these surfaces, and perform vertex-wise analyses. Additionally, myelin maps can be generated if both a T1w and T2w image is supplied. The subfield atlas includes the subiculum, cornu ammonis (CA) 1, CA2, CA3, CA4, and the dentate gyrus (DG). For more details refer to DeKraker et al. 40.

The original implementation of HippUnfold was designed for adult human data and thus may not perform well out-of-the box to other datasets, including neonate data. Therefore, two critical adjustments were made in the current study. First, the original implementation of HippUnfold uses a template defined on adult humans, which would be inappropriate for use on neonatal data. Thus, for the initial registration step a custom T1w template was created using a groupwise average template of all 638 neonatal participants used in this study. Similarly, the original nnU-Net in HippUnfold

was trained on adult human data, and thus the model is mismatched both in terms of image contrast (T1w images of neonates have grey and white matter contrast inverted), and anatomy. Performing manual segmentation of a large set of subjects from scratch to train a new model is a significant, arguably insurmountable, barrier, thus we made use of an iterative and incremental training paradigm to produce a new model. The process was seeded by a HippUnfold model (synthseg_v0.2) trained using a SynthSeg approach⁴¹, which used a set of ex vivo adult hippocampi to generate a large set of synthetic contrast MRI images, with randomized tissue contrast, to produce a model that is inherently agnostic to tissue contrast. This model was first applied to a set of 210 dHCP participants, and outputs were assessed visually by a trained expert, classifying each hippocampus as a success or failure. Successes were further characterized using a 5-point qualitative grading scheme defined by the extent of manual correction required, where grade 1 required extensive manual correction, and grade 5 required no manual correction. In this first segmentation iteration, 405 hippocampi completed segmentation, and there were 108 failures, and passing grades 1-5 were 11, 19, 54, 88, and 125, respectively. The grade 5 segmentations were used as-is, and the grade 3 and 4 segmentations were manually corrected, to provide a final set of 172 curated and corrected segmentations. The curated and corrected segmentations were used to train a new model from scratch using nnUnet, using the dHCP T1w images, which was denoted as neonateT1w_v2 in HippUnfold. To evaluate the effect of re-training, we performed quality control on the neonatal_T1w_v2 outputs of the same participants. This iteration resulted in 77 failures, and

Table 3 | Participant demographics and clinical characteristics

	Total data release	Final sample
N	783	520
Sex, n female (%)	359 (45.8%)	226 (43.5%)
n, preterm born (%)	205 (26.2%)	120 (23.1%)
Birth weight, kg, median (IQR)	3.2 (2.5–3.6)	3.2 (2.7–3.7)
Birth age, weeks, median (IQR)	39.3 (36.8–40.7)	39.6 (37.3–40.7)
Scan age, weeks, median (IQR)	40.9 (38.1–42.3)	40.9 (39.1–42.1)
n, longitudinal data (%)	104 (13.3%)	25 (4.8%)
Difference between birth and age at first scan, weeks, median (IQR)	1.1 (0.3–2.6)	0.9 (0.3–2.6)
Difference between birth and age at second scan, weeks, median (IQR)	9.6 (7.3–13.0)	8.6 (7.4–10.4)
n, congenital cardiac abnormality (%)	12 (1.5%) ^a	4 (0.8%)
n, congenital brain abnormality (%)	5 (0.6%) ^a	2 (0.4%)
n, congenital abnormality other than heart or brain (%)	5 (0.6%)	3 (0.6%)
n, necrotizing enterocolitis (%)	23 (2.9%)	10 (1.9%)
n, NICU stay	190	106
n, preterm born (%)	148 (77.9%)	85 (80.2%)
Days in NICU	19.0 (7.0–44.8)	18.0 (6.0–35.8)
n, received ventilation (%)	83 (43.7%)	45 (42.5%)
# days ventilation, median (IQR)	0.0 (0.0-2.8)	0.0 (0.0–2.0)

kg kilograms, NICU neonatal intensive care unit, IQR interquartile range.

passing grades 1–5 of 4, 5, 14, 25, and 295 respectively. This new model was applied to the remaining 428 infants, and the final success rate of the entire sample was 85%. The final neonate model is integrated and openly available within HippUnfold. Finally, T1w/T2w ratio maps were generated by HippUnfold using the –generate-myelin-maps flag, leveraging both the T1w and T2w images. While T1-weighted and T2-weighted MRI images do not convey information on myelination in isolation, taking the ratio of T1w to T2w signal intensity provides a proxy for myelin content within a tissue. This technique was first proposed and validated by Glasser and Van Essen³⁰. We did not consider the resolution sufficient to label the DG independently, thus we combined DG and CA4 into one label.

Statistics and reproducibility

All analyses were performed in R for statistical computing (https://www.rproject.org/), and code is available online at https://osf.io/8hte3/42. Both volumes and T1w/T2w ratio were analyzed using the same analytical method. The first analysis examined subfield measures in the cross-sectional sample (the "age" model), and a linear mixed model was constructed with postmenstrual age (i.e., age since conception) as a regressor, including a secondorder polynomial to determine whether the fit followed a quadratic shape. Sex and brain hemisphere were included as nuisance variables, and participant was included as a random effect. Marginal coefficients of determination (that is, R2) were calculated for each subfield's model, to estimate the variance explained by postmenstrual age. We then fit a second linear mixed model, using gestational age at birth and time since birth (that is, time spent both in utero and ex utero, the "stress" model accounting for preterm birth) as independent variables, again controlling for sex and brain hemisphere, with participant as a random effect. Marginal R² was computed. To determine which model provided a better fit, both R² values and tenfold cross validated mean squared error (MSE) were numerically compared for each subfield, and the model with the highest amount of variance explained, and the lower MSE, was considered the better fit (Table 1). As some infants had long periods between birth and being scanned, a sensitivity analysis was conducted to

determine whether eliminating outliers in this difference would produce similar results. The results are included in Table S1 in the Supplementary Information, and remain largely unchanged from the main analysis.

Next, we used the age and stress linear mixed effects models fit to the cross-sectional sample to predict the longitudinal data, to determine whether the age or stress model better predicted new data. Adjusted R² values were calculated for each subfield to determine how well both models fit the new data, and were again numerically compared to establish whether the age or stress model explained more variance (Table 1).

Finally, we analyzed the longitudinal sample. First, we examined the effect of term status on volumes and myelination, and whether preterm infants differed from term-born infants both at birth and once they reached full term. Term status refers to the age of the infant at the time of scan; if the infant was younger than 37 weeks, they were considered preterm. If the infant was born preterm but their scan was conducted after 37 weeks, they were considered term-equivalent. Finally, if the infant was born after 37 weeks, then they were considered term-born. In separate linear mixed effects models, subfield volumes and T1w/T2w ratios were analyzed, with term status as the independent variable, controlling for sex and hemisphere, with participant as a random effect.

Reporting summary

Further information on research design is available in the Nature Portfolio Reporting Summary linked to this article.

Data availability

The imaging and demographic data that support the findings of this study are available through the NIMH Data Archive under the title "Developing Human Connectome Project (dHCP)" collection ID #3955. Full Hippunfold code is available at http://github.com/khanlab/hippunfold. Volume and T1w/T2w ratio data and analysis code are available at https://osf.io/8hte3/.

Received: 21 January 2025; Accepted: 2 May 2025; Published online: 22 May 2025

References

- Lavenex, P. & Banta Lavenex, P. Building hippocampal circuits to learn and remember: insights into the development of human memory. Behav. Brain Res. 254, 8–21 (2013).
- Nichols, E. S. et al. Sex- and age-based differences in fetal and early childhood hippocampus maturation: a cross-sectional and longitudinal analysis. Cereb. Cortex 34, bhad421 (2024).
- Bauer, P. J., Pathman, T., Inman, C., Campanella, C. & Hamann, S. Neural correlates of autobiographical memory retrieval in children and adults. *Memory* 25, 450–466 (2017).
- May, J. C. et al. Event-related functional magnetic resonance imaging of reward-related brain circuitry in children and adolescents. *Biol. Psychiatry* 55, 359–366 (2004).
- Takashima, A., Bakker-Marshall, I., van Hell, J. G., McQueen, J. M. & Janzen, G. Neural correlates of word learning in children. *Dev. Cogn. Neurosci.* 37, 100649 (2019).
- Nichols, E. S., Blumenthal, A., Kuenzel, E., Skinner, J. K. & Duerden, E. G. Hippocampus long-axis specialization throughout development: a meta-analysis. *Hum. Brain Mapp.* 44, 4211–4224 (2023).
- Dahmen, B. et al. Effects of early-life adversity on hippocampal structures and associated HPA axis functions. *Dev. Neurosci.* 40, 13–22 (2017).
- Li, Y., Shen, M., Stockton, M. E. & Zhao, X. Hippocampal deficits in neurodevelopmental disorders. *Neurobiol. Learn Mem.* 165, 106945 (2019).
- Scheinost, D., Spann, M. N., McDonough, L., Peterson, B. S. & Monk, C. Associations between different dimensions of prenatal distress, neonatal hippocampal connectivity, and infant memory. Neuropsychopharmacology 45, 1272–1279 (2020).

^aOne infant had both a heart and a brain congenital abnormality.

- Kebaya, L. M. N. et al. Subcortical brain volumes in neonatal hypoxic-ischemic encephalopathy. *Pediatr. Res.* 94, 1797–1803 (2023).
- Bezanson, S., Nichols, E. S. & Duerden, E. G. Postnatal maternal distress, infant subcortical brain macrostructure and emotional regulation. *Psychiatry Res. Neuroimaging* 328, 111577 (2023).
- Krogsrud, S. K. et al. Development of hippocampal subfield volumes from 4 to 22 years. Hum. Brain Mapp. 35, 5646–5657 (2014).
- Aanes, S. et al. Reduced hippocampal subfield volumes and memory function in school-aged children born preterm with very low birthweight (VLBW). Neuroimage Clin. 23, 101857 (2019).
- Cole, J. H. et al. Subregional hippocampal morphology and psychiatric outcome in adolescents who were born very preterm and at term. *PLoS ONE* 10, e0130094 (2015).
- Hedderich, D. M. et al. Hippocampal subfield volumes are nonspecifically reduced in premature-born adults. *Hum. Brain Mapp.* 41, 5215–5227 (2020).
- Zeineh, M. M. et al. Direct visualization and mapping of the spatial course of fiber tracts at microscopic resolution in the human hippocampus. Cereb. Cortex 27, 1779–1794 (2017).
- Karat, B. G., DeKraker, J., Hussain, U., Köhler, S. & Khan, A. R. Mapping the macrostructure and microstructure of the in vivo human hippocampus using diffusion MRI. *Hum. Brain Mapp.* 44, 5485–5503 (2023).
- Wilson, S. et al. Development of human white matter pathways in utero over the second and third trimester. *Proc. Natl. Acad. Sci. USA* 118, 1–7 (2021).
- Grotheer, M. et al. Human white matter myelinates faster in utero than ex utero. Proc. Natl. Acad. Sci. 120, e2303491120 (2023).
- Chambers, J. S. & Perrone-Bizzozero, N. I. Altered myelination of the hippocampal formation in subjects with schizophrenia and bipolar disorder. *Neurochem. Res.* 29, 2293–2302 (2004).
- 21. Humphrey, T. The development of the human hippocampal fissure. *J. Anat.* **101**, 655 (1967).
- Ábrahám, H. et al. Myelination in the human hippocampal formation from midgestation to adulthood. *Int. J. Dev. Neurosci.* 28, 401–410 (2010)
- Lammertink, F. et al. Early-life stress exposure and large-scale covariance brain networks in extremely preterm-born infants. *Transl. Psychiatry* 12, 256 (2022).
- Lammertink, F., Vinkers, C. H., Tataranno, M. L. & Benders, M. J. N. L. Premature birth and developmental programming: mechanisms of resilience and vulnerability. *Front. Psychiatry* 11, 531571 (2021).
- Volpe, J. J. Dysmaturation of premature brain: importance, cellular mechanisms, and potential interventions. *Pediatr. Neurol.* 95, 42–66 (2019).
- Poeggel, G. et al. Juvenile emotional experience alters synaptic composition in the rodent cortex, hippocampus, and lateral amygdala. *Proc. Natl. Acad. Sci.* 100, 16137–16142 (2003).
- Reh, R. K. et al. Critical period regulation across multiple timescales. *Proc. Natl. Acad. Sci. USA* 117, 23242–23251 (2020).
- 28. Hughes, E. J. et al. A dedicated neonatal brain imaging system. *Magn. Reson Med.* **78**, 794–804 (2017).
- DeKraker, J., Ferko, K. M., Lau, J. C., Köhler, S. & Khan, A. R. Unfolding the hippocampus: an intrinsic coordinate system for subfield segmentations and quantitative mapping. *Neuroimage* 167, 408–418 (2018).
- Glasser, M. F. & Van Essen, D. C. Mapping human cortical areas in vivo based on myelin content as revealed by T1- and T2-weighted MRI. *J. Neurosci.* 31, 11597 (2011).
- Haast, R. A. M. et al. Insights into hippocampal perfusion using highresolution, multi-modal 7T MRI. *Proc. Natl. Acad. Sci. USA* 121, e2310044121 (2024).

- Bartsch, T., Döhring, J., Rohr, A., Jansen, O. & Deuschl, G. CA1 neurons in the human hippocampus are critical for autobiographical memory, mental time travel, and autonoetic consciousness. *Proc. Natl. Acad. Sci. USA* 108, 17562–17567 (2011).
- Roddy, D. W. et al. The hippocampus in depression: more than the sum of its parts? Advanced hippocampal substructure segmentation in depression. *Biol. Psychiatry* 85, 487–497 (2019).
- James, T. A. et al. Depression and episodic memory across the adult lifespan: a meta-analytic review. *Psychol. Bull.* 147, 1184–1214 (2021).
- Burnett, A. C. et al. Prevalence of psychiatric diagnoses in preterm and full-term children, adolescents and young adults: a meta-analysis. *Psychol. Med.* 41, 2463–2474 (2011).
- Cordero-Grande, L., Hughes, E. J., Hutter, J., Price, A. N. & Hajnal, J. V. Three-dimensional motion corrected sensitivity encoding reconstruction for multi-shot multi-slice MRI: application to neonatal brain imaging. *Magn. Reson Med.* 79, 1365–1376 (2018).
- Makropoulos, A. et al. The developing human connectome project: a minimal processing pipeline for neonatal cortical surface reconstruction. *Neuroimage* 173, 88–112 (2018).
- Kuklisova-Murgasova, M., Quaghebeur, G., Rutherford, M. A., Hajnal, J. V. & Schnabel, J. A. Reconstruction of fetal brain MRI with intensity matching and complete outlier removal. *Med. Image Anal.* 16, 1550–1564 (2012).
- Isensee, F., Jaeger, P. F., Kohl, S. A. A., Petersen, J. & Maier-Hein, K. H. nnU-Net: a self-configuring method for deep learning-based biomedical image segmentation. *Nat. Methods* 18, 203–211 (2021).
- DeKraker, J. et al. Automated hippocampal unfolding for morphometry and subfield segmentation with HippUnfold. *Elife* 11, e77945 (2022).
- Billot, B. et al. SynthSeg: segmentation of brain MRI scans of any contrast and resolution without retraining. *Med. Image Anal.* 86, 102789 (2023).
- Nichols, E. S. et al. Early life stress impairs hippocampal subfield myelination [Data set]. *Open Sci. Framework* https://doi.org/10. 17605/OSF.IO/8HTE3 (2025).

Author contributions

E.S.N. and E.G.D. designed the study. B.G.K. and A.F.K. led segmentation model training. E.S.N., B.G.K., M.G., and S.B. performed quality control of segmentations. E.S.N. led the data analysis and wrote the main manuscript, with contributions from all authors (B.G.K., M.G., S.B., A.F.K., E.G.D).

Competing interests

The authors declare no competing interests.

Additional information

Supplementary information The online version contains supplementary material available at https://doi.org/10.1038/s42003-025-08165-x.

Correspondence and requests for materials should be addressed to Emily S. Nichols.

Peer review information Communications Biology thanks the anonymous reviewers for their contribution to the peer review of this work. Primary Handling Editor: Benjamin Bessieres.

Reprints and permissions information is available at http://www.nature.com/reprints

Publisher's note Springer Nature remains neutral with regard to jurisdictional claims in published maps and institutional affiliations.

Open Access This article is licensed under a Creative Commons Attribution-NonCommercial-NoDerivatives 4.0 International License, which permits any non-commercial use, sharing, distribution and reproduction in any medium or format, as long as you give appropriate credit to the original author(s) and the source, provide a link to the Creative Commons licence, and indicate if you modified the licensed material. You do not have permission under this licence to share adapted material derived from this article or parts of it. The images or other third party material in this article are included in the article's Creative Commons licence, unless indicated otherwise in a credit line to the material. If material is not included in the article's Creative Commons licence and your intended use is not permitted by statutory regulation or exceeds the permitted use, you will need to obtain permission directly from the copyright holder. To view a copy of this licence, visit https://creativecommons.org/licenses/by-nc-nd/4.0/.

© The Author(s) 2025